




Impact of light sterile neutrinos on cosmological large scale structure

Rui Hu ^a, Ming-chung Chu ^a, Shek Yeung^a and Wangzheng Zhang ^a

^aDepartment of Physics, the Chinese University of Hong Kong, Sha Tin, Hong Kong SAR

E-mail: 1155168718@link.cuhk.edu.hk

Abstract. Sterile neutrinos with masses on the eV scale are promising candidates to account for the origin of neutrino mass and the reactor neutrino anomalies. The mixing between sterile and active neutrinos in the early universe could result in a large abundance of relic sterile neutrinos, which depends on not only their physical mass m_{phy} but also their degree of thermalization, characterized by the extra effective number of relativistic degrees of freedom ΔN_{eff} . Using neutrino-involved N-body simulations, we investigate the effects of sterile neutrinos on the matter power spectrum, halo pairwise velocity, and halo mass and velocity functions. We find that the presence of sterile neutrinos suppress the matter power spectrum and halo mass and velocity functions, but enhance the halo pairwise velocity. We also provide fitting formulae to quantify these effects.

Keywords: cosmological neutrinos, cosmological simulations, neutrino properties, power spectrum

Contents

1	Introduction	1
2	Theoretical and numerical aspects	4
2.1	Cosmic sterile neutrino background	4
2.2	Cosmological background evolution	4
2.3	Sterile neutrino free-streaming effect	4
3	Neutrino-involved N-body simulations	5
3.1	Standard test	5
3.2	Consistent simulations	6
4	Results	7
4.1	Sterile neutrino effects on matter power spectrum and two-point correlation function	7
4.2	Sterile neutrino effects on pairwise velocity	9
4.3	Effects on halo mass function and halo velocity function	12
5	Conclusions	14
A	Grid-based sterile neutrino-involved N-body simulations	15
A.1	Linear evolution of sterile neutrino over-density	15
A.2	Grid-based Method	16
B	Refitting of cosmological parameters: different sterile neutrino parameters	17
C	Cosmic variance	17

1 Introduction

Over the past several decades, a comprehensive and varied program of experimental neutrino measurements has significantly advanced our understanding of the elusive neutrino sector. This extensive research has uncovered findings that suggest the existence of physics beyond the Standard Model (SM), particularly the presence of non-zero neutrino masses, as evidenced by the discovery of neutrino flavor mixing. Furthermore, experimental results indicate that all observed neutrinos (antineutrinos) exhibit left-handed (right-handed) chirality¹ within experimental uncertainty. The existence of right-handed neutrinos provides a natural explanation to the small masses of neutrinos [2–4]. They do not participate in weak interactions and only interact gravitationally, thus called sterile neutrinos. This paper focuses on light sterile neutrinos with masses in the eV range.

The existence of the eV-scale sterile neutrinos is also motivated by experimental neutrino anomalies. Two short-baseline neutrino oscillation experiments, *LSND* [5] and *MiniBooNE* [6], found an excess of electron neutrinos from a muon neutrino beam. A potential solution

¹In Goldhaber’s experiment, the neutrinos’ helicities are determined by the helicities of γ ray emitted in the opposite direction of the neutrinos’ [1], but since neutrinos are relativistic, the chirality is approximately equal to helicity.

is to introduce an additional neutrino state with a mass of approximately 1 eV. Several short-baseline reactor neutrino experiments, *Daya Bay*, *MINOS+* and *Bugey-3* [7], have established a stringent exclusion on the sterile neutrino parameter space for $|\Delta m_{41}^2| < 1.2 \text{ eV}^2$. Additionally, the *MiniBooNE* experiment [8] also derives exclusion contours at the 95% C.L. in the planes of mass-squared splitting Δm_{41}^2 and the sterile neutrino mixing angles $\theta_{e\mu}$ and θ_{ee} , ruling out most of the parameter space suggested by the experimental anomalies. However, these experiments have not been able to impose a stringent exclusion for higher mass-squared splittings.

In addition to terrestrial experiments, cosmology offers another effective method for measuring the properties of sterile neutrinos. Relic eV-scale sterile neutrinos could be produced by neutrino oscillations in the early universe and behave like radiation. If the sterile neutrino state mixes sufficiently strongly with other neutrino states, there will be roughly equal numbers of sterile and SM neutrinos. Similar to active neutrinos, light sterile neutrinos delay the matter-radiation equality epoch, leaving distinct signatures on the cosmic microwave background (CMB). The number of relativistic degrees of freedom is usually parameterized by N_{eff} , defined so that the relativistic energy density after electron-positron annihilation is given by

$$\rho_{\text{rad}} = N_{\text{eff}} \frac{7}{8} \left(\frac{4}{11} \right)^{4/3} \rho_{\gamma}, \quad (1.1)$$

where ρ_{γ} is the photon energy density. The standard cosmological model has $N_{\text{eff}} \approx 3.046$, representing 3 types of active neutrinos², and $\Delta N_{\text{eff}} \equiv N_{\text{eff}} - 3.046$ denotes the extra relativistic degrees of freedom. Assuming the sum of 3 active neutrino mass eigenvalues $\sum m_i = 0.06 \text{ eV}$ with the normal hierarchy, the upper bounds $N_{\text{eff}} < 3.29$ and $m_{\text{eff}} < 0.65 \text{ eV}$ are obtained by fitting of Planck CMB and baryonic acoustic oscillation (BAO) data [11]. Here, $m_{\text{eff}} \equiv \Omega_{\nu_s} h^2 (94.1 \text{ eV})$ is the effective mass of sterile neutrino, characterizing its cosmological energy density Ω_{ν_s} . The physical mass of a sterile neutrino is $m_{\text{phy}} = (\Delta N_{\text{eff}})^{-1} m_{\text{eff}}$ when produced via the Dodelson mechanism [12]. The cosmological constraint on eV-scale sterile neutrinos can be relaxed by invoking non-standard cosmological production scenarios or introducing new neutrino interactions. For instance, by introducing the non-zero chemical potential of active neutrinos, BBN constraints allow $\Delta N_{\text{eff}} < 0.52$ [13]. Moreover, taking ΔN_{eff} to be 0.29 from CMB constraints, the mass bound becomes $m_{\text{phy}} < 2.24 \text{ eV}$. Hence, the eV-scale light sterile neutrinos cannot be completely ruled out. The degree of sterile neutrino thermalization quantified by ΔN_{eff} plays an important role in BBN and CMB constraints of sterile neutrino parameters.

In a later epoch, relic sterile neutrinos become non-relativistic. Nevertheless, sterile neutrinos stream freely, preventing them from clustering at scales smaller than their free-streaming length [14]. Structures below this range tend to be washed out due to the high velocity dispersion of sterile neutrinos, which imprints a distinct signature on large-scale structure (LSS). Combining local LSS surveys, such as galaxy shear power spectra from CFTHLenS surveys [15], SDSS Ly- α forest data [16], and X-ray *Chandra* observations [17], the constraints on sterile neutrino parameters are $m_{\text{eff}} < 0.22 \text{ eV}$ and $\Delta N_{\text{eff}} < 1.11$ (95% C.L.) [18].

Although combining Planck CMB data with future LSS data will not improve the constraint on ΔN_{eff} , it will significantly increase the sensitivity to m_{eff} . Combining CMB data

²Currently, N_{eff} is suggested to be 3.044 [9, 10]; here we keep the old value for consistency, which will have minimal impact on the results.

with galaxy and weak lensing data from Euclid [19] and DESI [20], the sensitivity could reach $m_{\text{eff}} < 60$ meV. Furthermore, future CMB experiments, such as CORE-M5, are expected to reach $m_{\text{eff}} < 37$ meV and $\Delta N_{\text{eff}} < 0.053$ [21].

An effective way to incorporate sterile neutrinos into N-body simulations is to treat them as an additional type of collisionless particles [22]. In addition to the bulk velocity, the sterile neutrino particles receive a thermal velocity from the Fermi-Dirac distribution. The same method can be used generally for hot dark matter (HDM). However, the resolution of sterile neutrinos or HDM particles should be at least twice of that CDM particles, which is computationally demanding. Another method to simulate sterile neutrinos uses a grid-based approach, treating sterile neutrinos as a linearly evolving background density [23, 24]. In this linear response approach (LRA), the sterile neutrino evolution is calculated semi-analytically, accounting for their interaction with the nonlinear dark matter field. This LRA makes the neutrino-involved simulation faster than the particle approach with the same accuracy. In this article, we construct our sterile neutrino-involved N-body simulation following the LRA approach.

Armed with high-resolution sterile neutrino-involved N-body simulations, one can investigate the impact of sterile neutrinos on various cosmological observables. For instance, it is well-known that light neutrinos suppress the matter power spectrum by $1 - 8\Omega_\nu/\Omega_m$, in a range of wave numbers k , giving rise to a spoon-shaped matter power spectrum due to free-streaming effects [25]. Here, Ω_ν and Ω_m denote the dimensionless energy densities of neutrinos and total matter, respectively. Sterile neutrinos may induce similar effects. The two-point correlation function (2PCF) is also an old but powerful tool for studying galaxy and matter clustering across different scales. It has contributed to significant discoveries, such as baryonic acoustic oscillations (BAO) [26], which serve as a reliable standard ruler due to their robustness against systematics [27]. Furthermore, 2PCF can be used to constrain various cosmological parameters [28–30].

The matter mean pairwise peculiar velocity, or pairwise velocity in short, denoted as $v_{12}(r)$, has also been used to constrain cosmological parameters, such as Ω_m and σ_8 [31–34], modified gravity [35], and kinematic Sunyaev-Zeldovich (kSZ) effects [36]. Both the pairwise velocity and its dispersion have been well studied [28, 37–39]. Besides, it can also be used to measure the neutrino mass and asymmetry [40].

The free-streaming effect of warm dark matter can also be revealed in halo statistics, such as the halo mass and velocity functions. The halo mass function (HMF) is sensitive to various cosmological parameters and baryonic physics [41, 42]. It is also useful for studying the impacts of massive neutrinos [43]. Similarly, the maximum circular velocity (MCV) of halos could also be related to the HMF [44] and the halo-galaxy connection [45, 46].

The article is organized as follows. Section 2 briefly reviews relic sterile neutrinos and elucidates our sterile neutrino-involved simulations. Section 3 presents convergence tests of our simulations and the cosmological parameters used. Section 4 discusses the impact of sterile neutrinos on various cosmology observables. We summarize our findings in Section 5. Appendices A, B, and C present the overview of our sterile neutrino-involved simulation method, the Markov-Chain Monte Carlo (MCMC) refitting results of cosmological parameters, and detailed tests, respectively.

2 Theoretical and numerical aspects

2.1 Cosmic sterile neutrino background

We assume that the cosmological sterile neutrinos maintain the same temperature as that of the relic standard model (SM) neutrinos, T_ν . The energy density of these SM neutrinos is

$$\rho_{\nu_a}(T_\nu) = 2 \times \frac{1}{2\pi^2} \sum_{i=1}^3 \int_0^\infty \frac{E_i}{\exp(E_i/T_\nu) + 1} p^2 dp, \quad (2.1)$$

where $E_i = \sqrt{p^2 + m_i^2}$ is the energy for SM neutrinos, with m_i the mass eigenvalues. The factor of 2 accounts for the antiparticles. Cosmic neutrinos decouple from the thermal bath at temperature $T_\nu \sim 1$ MeV, and the distribution has been frozen since then. Since neutrinos are still highly relativistic at $T_\nu \sim 1$ MeV, the E_i in the denominator in Eq. (2.1) can be simply replaced by the momentum p :

$$\rho_{\nu_a}(T_\nu) = 2 \times \frac{1}{2\pi^2} \sum_{i=1}^3 \int_0^\infty \frac{E_i}{\exp(p/T_\nu) + 1} p^2 dp. \quad (2.2)$$

Ref. [47] considered a 3 + 1 active-sterile neutrino system in the early universe with a full mixing matrix. The sterile neutrinos are not fully thermalized, but their distribution function follows

$$f_{\nu_s}^0 = \frac{1}{2\pi^2} \frac{\Delta N_{\text{eff}}}{\exp(p/T_\nu) + 1}. \quad (2.3)$$

2.2 Cosmological background evolution

We start with the deviation of the Hubble expansion history from that of the standard Λ CDM universe. The Hubble expansion rate is determined by the Friedmann equation including neutrinos,

$$H^2(a) \equiv \left(\frac{\dot{a}}{a}\right)^2 = H_0^2(\Omega_{\gamma,0}a^{-4} + \Omega_{cb,0}a^{-3} + \Omega_\Lambda + \Omega_{\nu_a}(a) + \Omega_{\nu_s}(a)), \quad (2.4)$$

where $\Omega_{\gamma,0}$, $\Omega_{cb,0}$, and Ω_Λ are the current energy densities of photons, cold dark matter plus baryonic matter, and dark energy, respectively, and $H_0 = H(a = 1)$. The evolution of active and sterile neutrino energy densities, Ω_{ν_a} and Ω_{ν_s} , can be calculated using their distribution functions, such as Eq. (2.3).

2.3 Sterile neutrino free-streaming effect

After decoupling, neutrinos stream freely. Similar to active neutrinos, cosmological sterile neutrinos are only weakly bound by the gravitational potential below the free-streaming scale because of their high thermal speeds. When sterile neutrinos become non-relativistic during matter domination, the free-streaming length is given by [14]

$$\lambda_{\text{fs}} \approx 8.10(1+z) \frac{H_0}{H(z)} \left(\frac{1 \text{ eV}}{m_{\text{phy}}}\right) h^{-1} \text{ Mpc}. \quad (2.5)$$

Due to free-streaming effects, the growth of 3+1 neutrino over-density δ_ν is much slower than that of CDM plus baryonic matter δ_{cb} , which leads to a smaller total matter over-density field δ_t than that in the Λ CDM model due to the averaging effect:

$$\delta_t = (1 - f_\nu)\delta_{cb} + f_\nu\delta_\nu = (1 - f_\nu)\delta_{cb} + f_{\nu_a}\delta_{\nu_a} + f_{\nu_s}\delta_{\nu_s}, \quad (2.6)$$

	T0	T1	T2	T3	T4
$m_{\text{phy}}[\text{eV}]$	0	1	1	2	2
ΔN_{eff}	0	0.2	0.4	0.2	0.4
$m_{\text{eff}}[\text{eV}]$	0	0.2	0.4	0.4	0.8

Table 1. Combinations of m_{phy} and ΔN_{eff} with fixed cosmological parameters. Here, m_{phy} is the physical mass of the sterile neutrinos and $m_{\text{eff}} \equiv m_{\text{phy}} \cdot \Delta N_{\text{eff}}$ is the corresponding effective mass.

where $f_\nu = (\Omega_{\nu_a} + \Omega_{\nu_s})/\Omega_m = f_{\nu_a} + f_{\nu_s}$ is the ratio between energy densities of 3+1 neutrinos and total matter. δ_{ν_a} (δ_{ν_s}) is the active (sterile) neutrino over-density. Hence, in cosmological simulations, the total matter density field can be written as

$$\tilde{\rho}_t(\mathbf{k}) = \tilde{\rho}_{\text{cb}}(\mathbf{k}) + \tilde{\rho}_{\text{cb}}(\mathbf{k}) \frac{f_\nu}{1 - f_\nu} \times \frac{\delta_\nu}{\delta_{\text{cb}}}, \quad \frac{\delta_\nu}{\delta_{\text{cb}}} \approx \left(\frac{P_\nu(\mathbf{k})}{P_{\text{cb}}(\mathbf{k})} \right)^{1/2}, \quad (2.7)$$

where $P_\nu(\mathbf{k})$ and $P_{\text{cb}}(\mathbf{k})$ are the 3 + 1 neutrino power spectrum and CDM-baryon power spectrum, respectively. Similar to that for active neutrinos [48], the linear growth equation of the sterile neutrino over-density field is

$$\begin{aligned} \tilde{\delta}_{\nu_s} = & \tilde{\delta}_{\nu_s}(s_i, \mathbf{k}) \Phi[\mathbf{k}(s - s_i)] [1 + (s - s_i) a_i^2 H(a_i)] + 4\pi G \int_{s_i}^s a^4 (s - s') \Phi[\mathbf{k}(s - s')] \\ & \times \left[\bar{\rho}_{\text{cb}}(s') \delta_{\text{cb}}(s', \mathbf{k}) + \sum_i \bar{\rho}_{\nu_i}(s') \delta_{\nu_i}(s', \mathbf{k}) + \bar{\rho}_{\nu_s}(s') \delta_{\nu_s}(s', \mathbf{k}) \right] ds', \end{aligned} \quad (2.8)$$

where s is the comoving time defined in Eq. (A.4), $\tilde{\delta}_{\nu_i}$ and $\tilde{\delta}_{\nu_s}$ are over-density fields of the 3 active neutrinos and sterile neutrinos in k -space, respectively, and

$$\Phi(\mathbf{q}) \equiv \frac{\int f_{\nu_s}^0(\mathbf{p}) e^{-i\mathbf{q}\cdot\mathbf{p}} d^3\mathbf{p}}{\int f_{\nu_s}^0(\mathbf{p}) d^3\mathbf{p}}. \quad (2.9)$$

The derivation of Eqs. (2.8) and (2.9) is shown in Appendix A.1. The grid-based sterile neutrino-involved N-body simulations are similar to the method presented in [48]. Appendix A.2 overviews the details of the simulation procedure.

3 Neutrino-involved N-body simulations

3.1 Standard test

In our simulations, active neutrinos with 3 degenerate masses are considered with total mass $\sum m_{\nu_i} = 0.06 \text{ eV}$. We have modified **Gadget-2** [49] to incorporate both active and sterile neutrinos. The initial conditions are generated by **2LPTic** [50], incorporating the active and sterile neutrino effects in the Friedmann equation. The initial power spectrum of CDM plus baryons and 3 + 1 neutrinos at $z = 99$ are calculated using **CAMB**³ [51]. For validation of the simulation, we studied 5 cases, with different combinations of m_{phy} and ΔN_{eff} shown in Table 1. The background cosmology is fixed using Planck18 best-fit cosmological parameters [11] so that the total matter density and baryon density are the same. The active and sterile neutrino densities are subtracted from the CDM density. The simulations are conducted

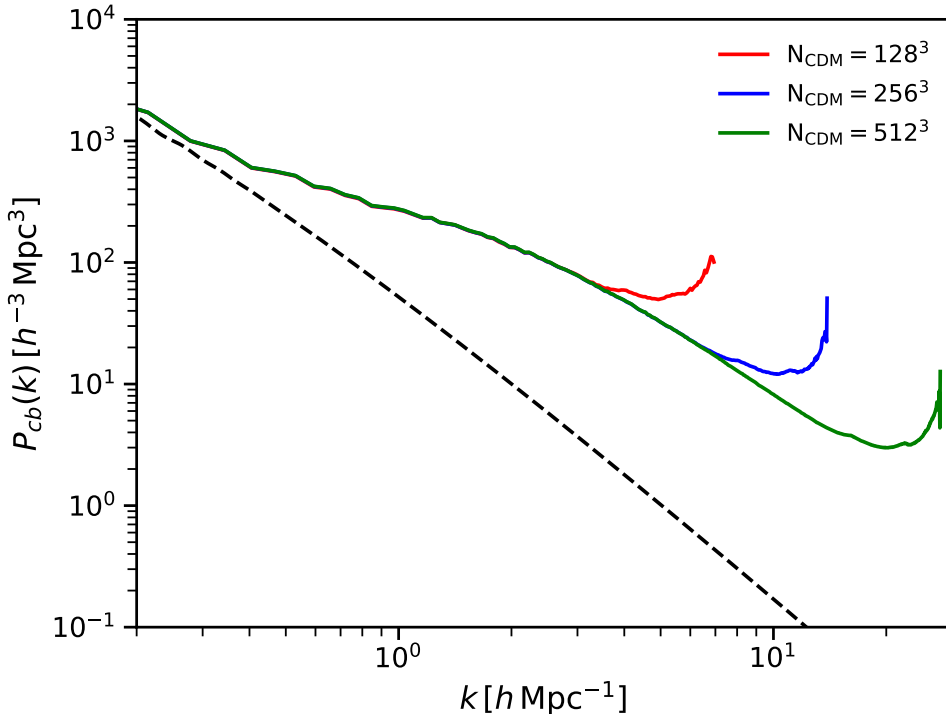


Figure 1. Power spectra of CDM plus baryons with different resolutions at redshift $z = 0$. The solid lines with different colors show the simulation results with different resolutions. The dashed black line presents the linear power spectrum of CDM plus baryons for reference.

within a boxsize of $100h^{-1}$ Mpc, comprising $N_{\text{CDM}} = 128^3$ CDM particles. For the convergence test, T1 is run with $N_{\text{CDM}} = 128^3, 256^3, 512^3$. As shown in Figure 1, the results of neutrino-involved simulations converge well. With a fixed cosmology, the power spectrum of CDM plus baryons has a spoon-shape suppression at $k \sim 1h \text{ Mpc}^{-1}$ impacted by sterile neutrinos as seen in Figure 2, which is similar to the effect seen with active neutrinos.

3.2 Consistent simulations

To study the effects of sterile neutrinos on cosmic structure evolution, we use the same combinations of m_{phy} and ΔN_{eff} in Table 1, but the other cosmological parameters are derived via refitting, utilizing the `Cosmomc`⁴ software [52], of the Planck 2018 `plikHM_TTTEEE` and BAO data [11, 26]. Detailed cosmological parameters are shown in Table 2. $N_{\text{CDM}} = 1024^3$ and boxsize $L = 1000 h^{-1}$ Mpc are used. Dark matter halos are identified using the `Rockstar`⁵ software [53], which employs adaptive hierarchical refinement of friends-of-friends groups in phase-space dimensions, and analyses are conducted across multiple redshifts.

³<https://camb.info/>

⁴<https://cosmologist.info/cosmomc/>

⁵<https://bitbucket.org/gfcstanford/rockstar/src/main/>

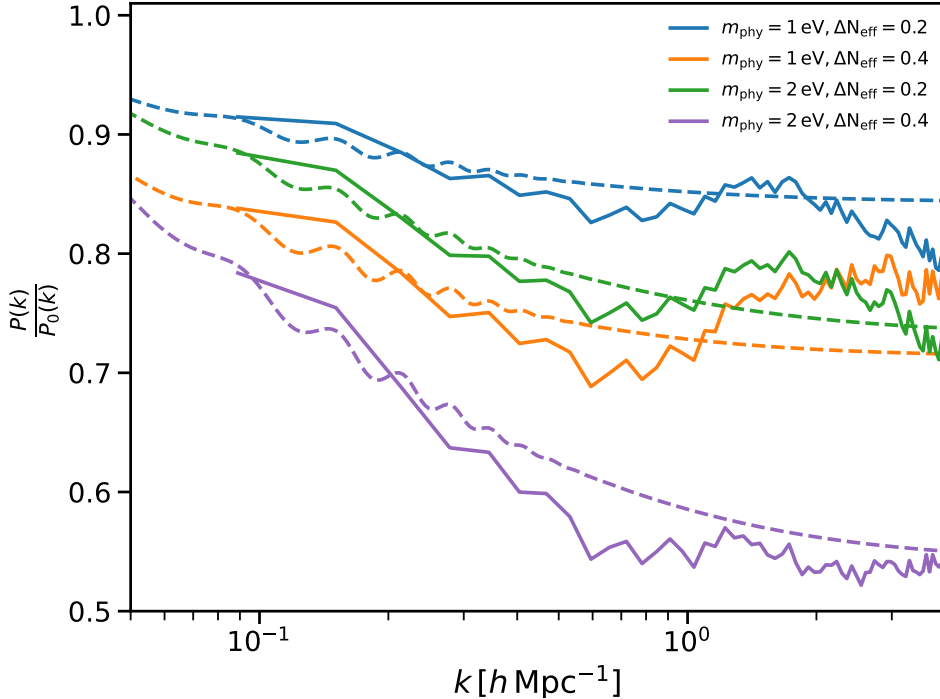


Figure 2. Ratios of total matter power spectra for T1, T2, T3, and T4 to that of T0 at redshift $z = 0$, in linear theory (dashed lines) and simulations (solid lines).

	$m_{\text{phy}}[\text{eV}]$	ΔN_{eff}	$H_0[\text{km s}^{-1}\text{Mpc}^{-1}]$	$\Omega_c h^2$	$\Omega_b h^2$	Ω_Λ	n_s	$\ln A_s$
A0	0	0	67.75	0.1193	0.0224	0.6897	0.967	3.046
B1	1	0.2	67.90	0.1215	0.0226	0.6814	0.973	3.062
B2	1	0.4	68.11	0.1236	0.0228	0.6739	0.979	3.078
C1	2	0.2	67.46	0.1199	0.0226	0.6760	0.970	3.063
C2	2	0.4	67.27	0.1204	0.0228	0.6631	0.974	3.082

Table 2. Combinations of m_{phy} and ΔN_{eff} and the corresponding refitted cosmological parameters.

4 Results

4.1 Sterile neutrino effects on matter power spectrum and two-point correlation function

We analyze the matter power spectrum utilizing the `Pylians` software [54]. Figure 3 shows the total matter power spectra and their fractional deviations from that of the fiducial case (A0) for different combinations of m_{phy} and ΔN_{eff} ,

$$R(k) = \Delta P(k)/P_0(k) = \frac{P(k) - P_0(k)}{P_0(k)}, \quad (4.1)$$

showing a suppression of around 10% already for $m_{\text{phy}} = 1 \text{ eV}$ with $\Delta N_{\text{eff}} = 0.2$. Although increasing m_{phy} or ΔN_{eff} will suppress the matter power spectrum, their degeneracy cannot

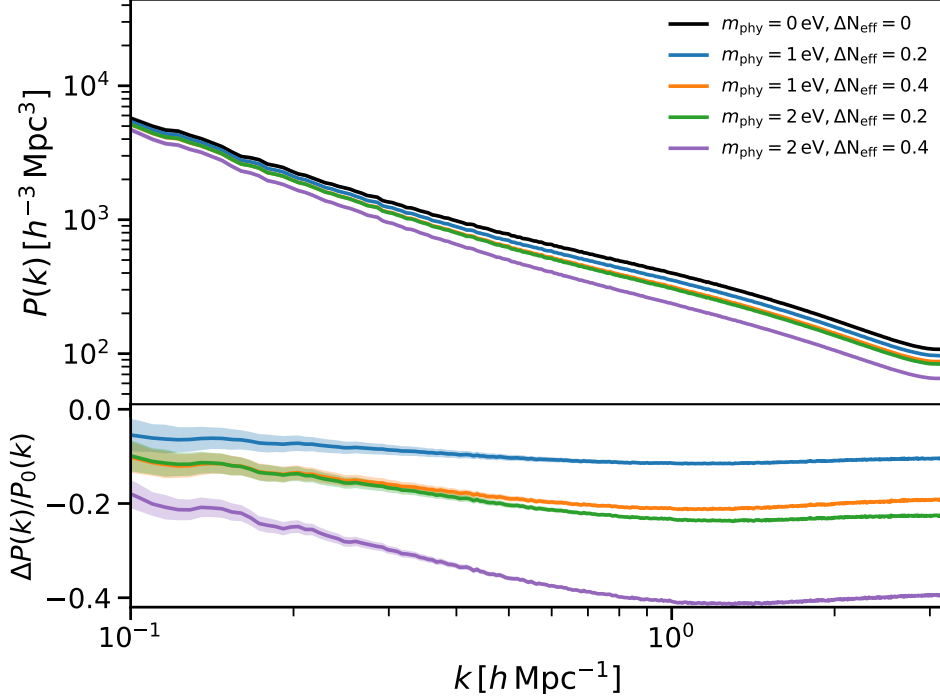


Figure 3. Total matter power spectra (upper panel) and fractional deviations (lower panel) with respect to the fiducial case A0 for different combinations of m_{phy} and ΔN_{eff} . Shaded regions show the statistical errors.

be represented by m_{eff} alone. For example, even though the combinations B2 and C1 have the same $m_{\text{eff}} = m_{\text{phy}} \cdot \Delta N_{\text{eff}}$, their total matter power spectra differ by a few percent. To quantify the effects of sterile neutrinos, we take $R(k)$ averaged over the range of $[0.7, 2.5] h \text{ Mpc}^{-1}$, yielding

$$\bar{R} = \frac{\sum R(k)}{N_{\text{kbin}}}, \quad (4.2)$$

where N_{kbin} is the number of k_i bins sampled in this range. \bar{R} can be fitted by expanding $\bar{R}(m_{\text{phy}}, \Delta N_{\text{eff}})$ at the fiducial values $m_{\text{phy}} = 0, \Delta N_{\text{eff}} = 0$ (A0) and keeping the lowest order terms:

$$\begin{aligned} \bar{R}(m_{\text{phy}}, \Delta N_{\text{eff}}) = & C_{mm} \cdot \left(\frac{m_{\text{phy}}}{1 \text{ eV}}\right)^2 + C_{nn} \cdot (\Delta N_{\text{eff}})^2 + C_{mn} \cdot \frac{m_{\text{phy}}}{1 \text{ eV}} \times \Delta N_{\text{eff}} \\ & + C_m \cdot m_{\text{phy}} + C_n \cdot \Delta N_{\text{eff}}, \end{aligned} \quad (4.3)$$

where $C_{mm}, C_{nn}, C_{mn}, C_m$ and C_n are expansion coefficients. When ΔN_{eff} is equal to 0, there is no sterile neutrinos effects on the matter power spectrum, so $\bar{R}(m_{\text{phy}}, \Delta N_{\text{eff}} = 0) = 0$. Therefore, the fitting formula can be simplified as:

$$\bar{R}(m_{\text{phy}}, \Delta N_{\text{eff}}) = C_{nn} \cdot (\Delta N_{\text{eff}})^2 + C_{mn} \cdot \frac{m_{\text{phy}}}{1 \text{ eV}} \times \Delta N_{\text{eff}} + C_n \cdot \Delta N_{\text{eff}}. \quad (4.4)$$

The fitted parameters are $C_{nn} = 0.472 \pm 0.177$, $C_{mn} = -0.522 \pm 0.028$, and $C_n = -0.169 \pm 0.078$. The results are shown in Figure 4.

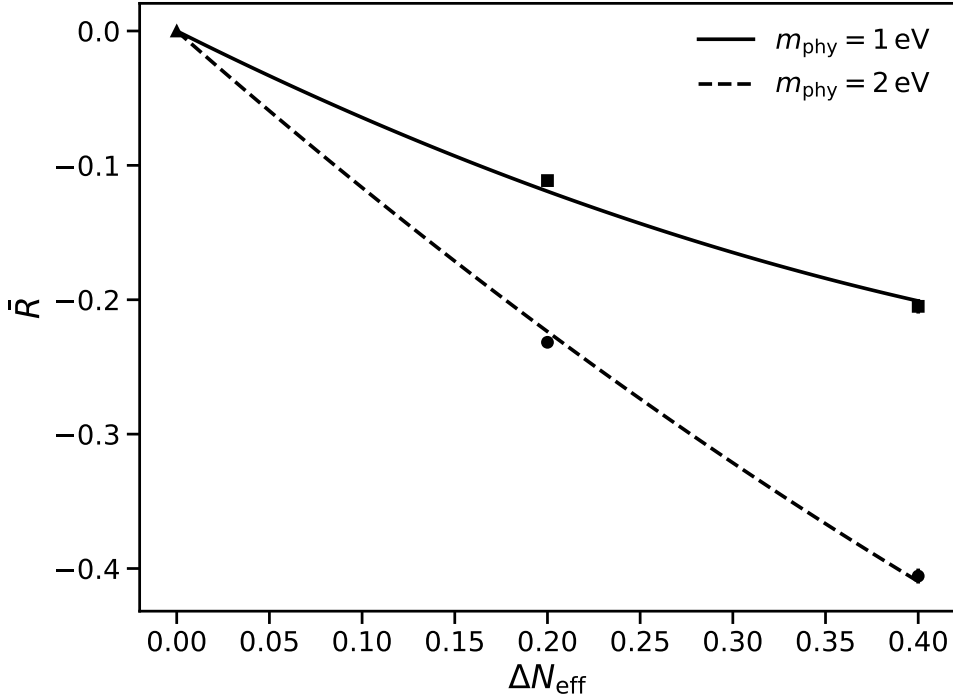


Figure 4. Fractional deviations of the matter power spectrum from that of A0 (triangle) averaged over the range $k \in [0.7, 2.5] h \text{ Mpc}^{-1}$ for $m_{\text{phy}} = 1 \text{ eV}$ (squares) and 2 eV (circles). The dashed and solid lines are the fitting results.

Since many catalogs list the positions of galaxies or galaxy clusters, it is useful to study the matter spatial distribution. Besides the matter power spectrum, we also calculate the two-point correlation function,

$$\xi(r) = \langle \delta_{cb}(\mathbf{r}') \delta_{cb}(\mathbf{r}' + \mathbf{r}) \rangle. \quad (4.5)$$

One can estimate $\xi(r)$ through the pair counts of particle points and random points [55],

$$\xi(r) = \frac{DD - 2DR + RR}{RR}, \quad (4.6)$$

where DD , DR , and RR are the normalized numbers of particle-particle pairs, particle-random pairs, and random-random pairs, respectively. A simple estimate of the statistical error assumes that the number of independent pairs in a given r bin follows a Poisson distribution.

Figure 5 shows that $\xi(r)$ is suppressed for increasing m_{phy} or ΔN_{eff} by up to around 30% in the case of C2. The degeneracy of the two parameters is broken at $r < 4 h^{-1} \text{ Mpc}$, which is consistent with the results from the matter power spectrum.

4.2 Sterile neutrino effects on pairwise velocity

The velocity field also carries half of the phase-space information of cosmological structures. In this section, we focus on the pairwise velocity and its dispersion. The pairwise velocity

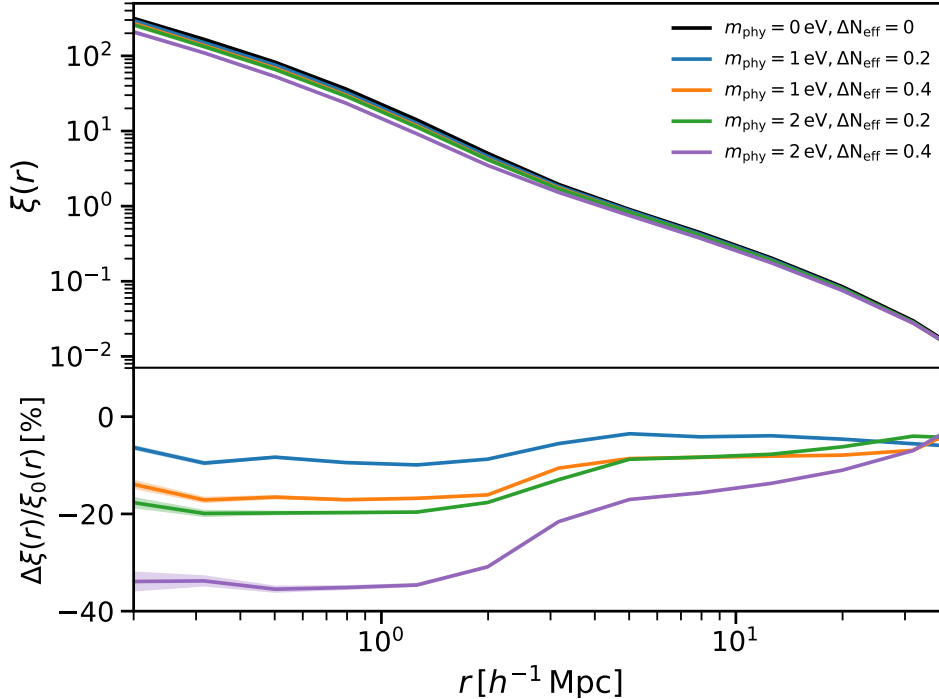


Figure 5. Same as Figure 3, but for the two-point correlation function.

v_{12} is defined as the peculiar velocity difference of a pair of objects projected along their line of separation, averaged over all pairs at separation r [56],

$$v_{12}(r) \equiv \langle (\mathbf{v}_1 - \mathbf{v}_2) \cdot \hat{\mathbf{r}} \rangle, \quad (4.7)$$

where $\hat{\mathbf{r}} = (\mathbf{r}_1 - \mathbf{r}_2) / |\mathbf{r}_1 - \mathbf{r}_2|$ and $\mathbf{v}_{1,2}$ is the peculiar velocity of object 1 and 2, respectively. The pairwise velocity v_{12} shows the tendency of two objects to move closer ($v_{12} < 0$) or farther apart ($v_{12} > 0$) from each other. The pairwise velocity dispersion

$$\sigma_{12}(r) = \langle [(\mathbf{v}_1 - \mathbf{v}_2) \cdot \hat{\mathbf{r}}]^2 \rangle^{1/2} \quad (4.8)$$

describes the r.m.s. fluctuations of v_{12} . Both v_{12} and σ_{12} help us understand how objects such as galaxies move relative to each other due to their gravitational interactions.

The pairwise velocity can be estimated analytically. For an evolving point distribution, the averaged number of neighbors within a comoving distance r of an object is

$$N(r, t) = 4\pi\bar{n}(t)a^3 \int_0^r [1 + \xi(r', a)] r'^2 dr', \quad (4.9)$$

where $\bar{n}(t)$ is the mean object number density at time t and $\xi(r, a)$ is the two-point correlation function at scale factor a [57]. The conservation of mass can be expressed as

$$\frac{\partial N(r, t)}{\partial t} + 4\pi\bar{n}a^2 r^2 [1 + \xi(r, a)] v_{12} = 0. \quad (4.10)$$

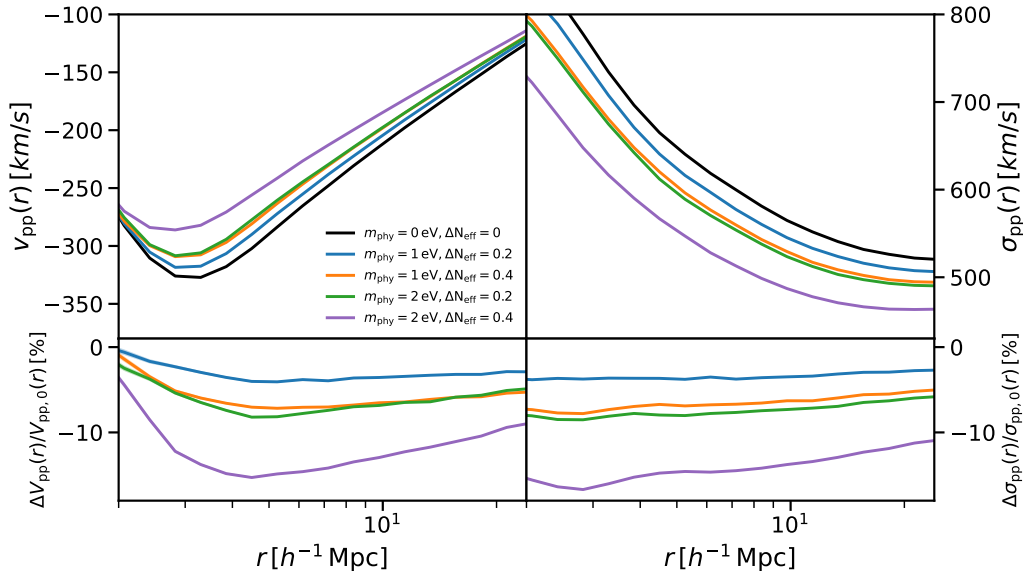


Figure 6. Particle-particle pairwise velocities (upper left) and dispersions (upper right) for different sterile neutrino parameter combinations and their fractional deviations with respect to A0 (lower panels).

Combining Eq. (4.9) and Eq. (4.10), we have

$$v_{12}(r, a) = -\frac{H(a)a^2}{[1 + \xi(r, a)]r^2} \frac{\partial}{\partial a} \int_0^r \xi(r', a)r'^2 dr'. \quad (4.11)$$

For large separation r where $\xi(r, a) \ll 1$, $\xi(r, a)$ can be expanded to the first order as $\xi(r, a) = \xi(r, 1)D^2(a)$, with $D(a)$ the linear growth factor. Hence, Eq. (4.11) is written as

$$v_{12}(r, a) = -\frac{2}{3}Hra f(a) \frac{3 \int_0^r \xi(r', a)r'^2 dr'}{r^3 [1 + \xi(r, a)]}, \quad (4.12)$$

where $f(a) \equiv d \ln D / d \ln a$ is the linear growth rate. To good approximation, $f(a) \approx \Omega_m^{0.55}$ [58].

Figure 6 displays the particle-particle pairwise velocity v_{pp} and dispersion σ_{pp} as well as their corresponding fractional deviations from the fiducial case, $(v_{pp} - v_{pp,0})/v_{pp,0}$ and $(\sigma_{pp} - \sigma_{pp,0})/\sigma_{pp,0}$, with uncertainties staying within 1%. Both v_{pp} and σ_{pp} decrease in magnitude for larger m_{phy} or ΔN_{eff} , showing that particles are less attracted by each other. The deviations of pairwise velocity from that of A0 can be well parameterized by $m_{\text{eff}} \equiv m_{\text{phy}} \cdot \Delta N_{\text{eff}}$. For example, B2 and C1, which have the same value of m_{eff} , show similar v_{pp} and σ_{pp} .

We select halos in the mass range of $[10^{13}, 10^{14}] \text{Mpc } h^{-1}$ to calculate the halo-halo pairwise velocity v_{hh} and dispersion σ_{hh} . Here, the distinct host halos are considered, which contain at least one bound halo as the main halo located at the center, with each halo composing of at least 200 CDM particles. The halo mass M_{200c} is defined as the mass of CDM particles contained within a radius R_{200c} enclosing a mean over-density of 200 times the critical density. Figure 7 displays v_{hh} and σ_{hh} their fractional deviations from those of the

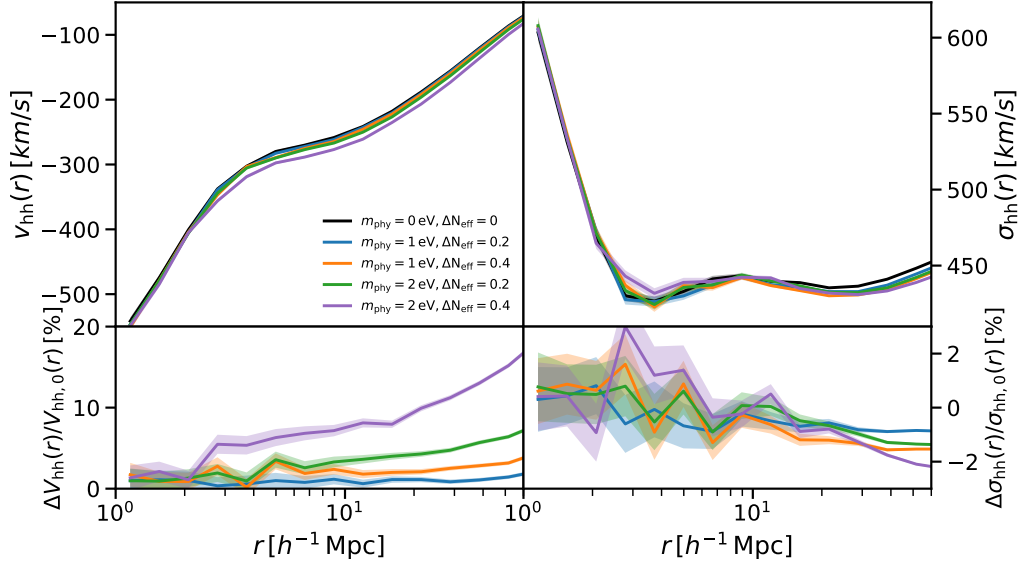


Figure 7. Same as Figure 6, but for halo pairs.

Table 3. Fitting results of \bar{R}_{hh}^v and $\bar{R}_{\text{hh}}^\sigma$ for $M_h \in [10^{13}, 10^{14}] M_\odot h^{-1}$ at the range $[6, 20] \text{ Mpc } h^{-1}$.

quantity	$C_{nn}^{v/\sigma}$	$C_{mn}^{v/\sigma}$	$C_n^{v/\sigma}$
v_{hh}	0.034 ± 0.027	0.134 ± 0.006	-0.097 ± 0.012
σ_{hh}	0.041 ± 0.005	0.014 ± 0.001	-0.052 ± 0.002

fiducial case A0, $\bar{R}_{\text{hh}}^v = (v_{\text{hh}} - v_{\text{hh},0})/v_{\text{hh},0}$ and $\bar{R}_{\text{hh}}^\sigma = (\sigma_{\text{hh}} - \sigma_{\text{hh},0})/\sigma_{\text{hh},0}$. For $r > 4 \text{ Mpc } h^{-1}$, $|v_{\text{hh}}|$ increases as m_{phy} or ΔN_{eff} increases, while σ_{hh} decreases. Similar to the total matter power spectrum, we take the averaged fractional deviations $\bar{R}_{\text{hh}}^{v/\sigma}$ of v_{hh} and σ_{hh} over the range $[6, 20] \text{ Mpc } h^{-1}$, and provide a fitting formula:

$$\bar{R}_{\text{hh}}^{v/\sigma}(m_{\text{phy}}, \Delta N_{\text{eff}}) = C_{nn}^{v/\sigma} \cdot (\Delta N_{\text{eff}})^2 + C_{mn}^{v/\sigma} \cdot \frac{m_{\text{phy}}}{1 \text{ eV}} \times \Delta N_{\text{eff}} + C_n^{v/\sigma} \cdot \Delta N_{\text{eff}}. \quad (4.13)$$

The fitted coefficients are presented in Table 3.

4.3 Effects on halo mass function and halo velocity function

We have shown that CDM structures are impacted by the presence of sterile neutrinos through the suppression and enhancement of the matter power spectrum and pairwise velocity, respectively. On the other hand, the statistics of CDM halos can also be used to constrain models. In this section, we investigate the impact of sterile neutrinos on the CDM halo statistics.

Now we will discuss the HMF for different sterile neutrino parameters. The HMF shows the mass distribution of dark matter halos, giving the number density of halos n in each mass

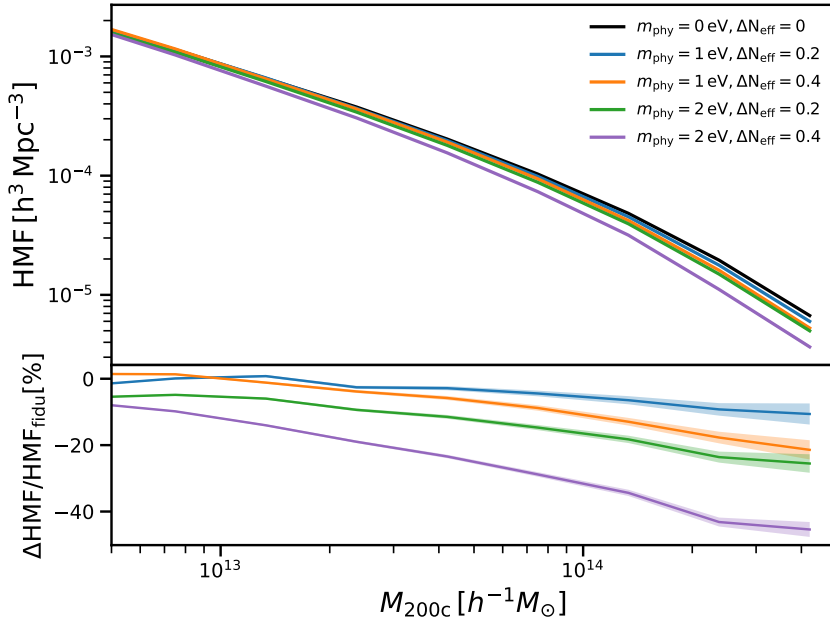


Figure 8. Same as Figure 3, but for halo mass function.

bin. We parameterize it in the following way:

$$\text{HMF}(M_{200c}) \equiv \frac{dn}{d \log M_{200c}} = T(\sigma, z) \frac{\rho}{M_{200c}} \frac{d \log \sigma^{-1}(M, z)}{d M_{200c}}, \quad (4.14)$$

where $\frac{dn}{d \log M_{200c}}$ is the comoving number density of dark matter halos per unit mass (in log basis) at redshift z , ρ is the mean density of the CDM and baryons, and

$$\sigma^2 = \frac{1}{2\pi^2} \int_0^\infty k^2 P(k, z) W^2(k, R_{200c}) dk, \quad (4.15)$$

with $P(k, z)$ being the total matter power spectrum at z and $W(k, R_{200c})$ the top-hat window function with radius R_{200c} . $T(\sigma, z)$ is a factor that can be well-fitted by the Sheth-Tormen approximation in the Λ CDM model [59]. Figure 8 displays the HMFs for different sterile neutrino parameter combinations. Despite the uncertainties, the HMF is reduced for increasing m_{phy} or ΔN_{eff} , and the reduction increases at the high-mass end as expected, which is similar to the suppression found with active neutrinos [60]. For instance, the suppression of the HMF is up to 40-50% for $m_{\text{phy}} = 2 \text{ eV}$ and $\Delta N_{\text{eff}} = 0.4$ compared to the fiducial case A0, showing the sterile neutrino effect to delay the structure formation or smooth out structures. Moreover, different combinations of m_{phy} and ΔN_{eff} with the same m_{eff} (B2 and C1) exhibit different strengths of reduction.

The maximum circular velocity is another tool to characterize halos [61–63], which is defined as

$$V_{\text{circ}} = \sqrt{\frac{GM_{<r}}{r}} \Big|_{\text{max}}, \quad (4.16)$$

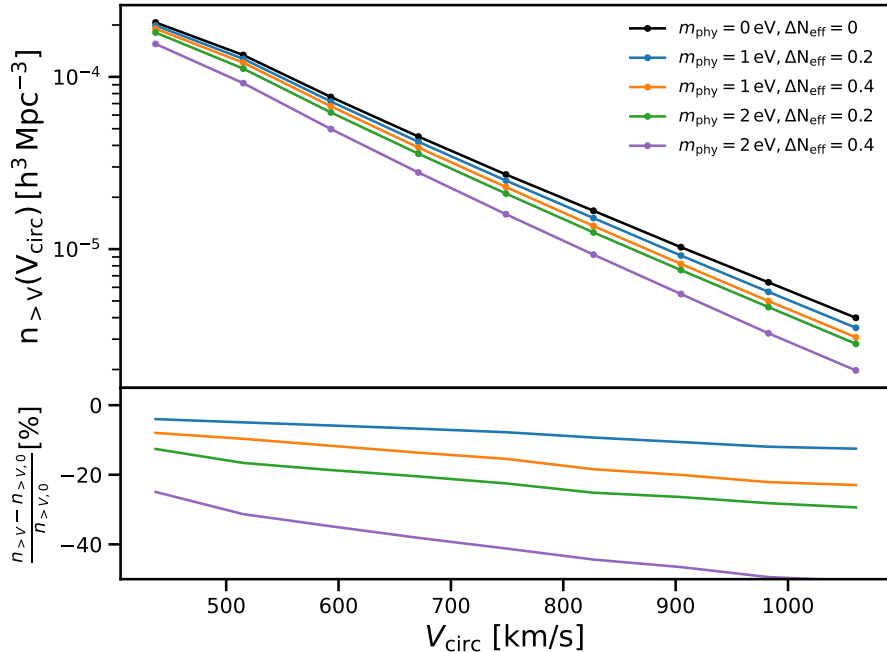


Figure 9. Same as Figure 3, but for cumulative halo velocity function.

where $M_{<r}$ is the enclosed mass within radius r and “max” indicates the maximum circular velocity. The MCV is reached in the central halo region, which is expected to correlate better with the stellar or luminous component and be less sensitive to tidal stripping. Figure 9 displays the cumulative velocity function, $n_{>V}(V_{\text{circ}})$, which represents the number density of dark matter halos with a circular velocity larger than V_{circ} . The cumulative velocity function is reduced for larger m_{phy} and ΔN_{eff} . This reduction increases with V_{circ} and reaches around 50% at the high-speed end for the case C2. Compared to the HMF, the parameter degeneracy (between B2 and C1) is broken more for the cumulative velocity function.

5 Conclusions

In this paper, we present the sterile neutrino effects on the matter power spectrum, pairwise velocity, and dark matter halo statistics calculated using sterile neutrino-involved cosmological simulations. The correction of gravitational potential due to sterile and active neutrinos is calculated through the PM grid method. The sterile neutrino over-density responds to the nonlinear CDM plus baryon density according to the linear theory. This evolution equation may also describe other decoupled particles whose over-densities are small. For instance, similar to the neutrinos, the cosmic QCD axions with eV masses have significant thermal velocities and their over-densities are also small. More interestingly, they may have a Fermi-Dirac-shaped distribution through thermal production after decoupling [64]. In this case, the eV-scale QCD axions can also be studied using this cosmological simulation. The simulations converge well with respect to resolutions.

To consistently investigate the impact of sterile neutrinos on the large-scale structure, we run the simulations with cosmological parameters refitted with the Planck CMB and BAO data for each set of $\{m_{\text{phy}}, \Delta N_{\text{eff}}\}$. Our key conclusions are summarized below.

- (i) For the large-scale spatial information, the total matter power spectrum and two-point correlation function are studied. Both of these are suppressed by up to around 40% for $m_{\text{eff}} = 0.8 \text{ eV}$ compared to the fiducial case with no sterile neutrinos. The degeneracy between effects of m_{phy} and ΔN_{eff} is broken for $k \gtrsim 1h \text{ Mpc}^{-1}$. A fitting formula for the averaged fractional deviations of total matter power spectrum is presented.
- (ii) We calculate the halo-halo pairwise velocity and its dispersion, showing the tendency for objects to be attracted by each other. The halo-halo pairwise velocity (dispersion) increases (decreases) in magnitude by up to 15% (2%) as m_{phy} or ΔN_{eff} increases for halos in the mass range $[10^{13}, 10^{14}] M_{\odot} h^{-1}$. Similar to the matter power spectrum, we present the fitting formulae for the averaged fractional deviations of v_{hh} and σ_{hh} .
- (iii) The presence of sterile neutrinos suppresses the halo mass and cumulative circular velocity functions by up to 40-50% for $m_{\text{eff}} = 0.8 \text{ eV}$. These fractional deviations are larger at their high-mass and high-speed ends.

A Grid-based sterile neutrino-involved N-body simulations

A.1 Linear evolution of sterile neutrino over-density

This section briefly overviews the linear evolution of sterile neutrino over-density, following previous neutrino studies [23, 40, 48, 65]. Starting with the Vlasov equation for the sterile neutrinos,

$$\frac{dF_{\nu_s}}{dt} = \frac{\partial F_{\nu_s}}{\partial t} + \dot{\mathbf{r}} \cdot \frac{\partial F_{\nu_s}}{\partial \mathbf{r}} + \dot{\mathbf{v}} \cdot \frac{\partial F_{\nu_s}}{\partial \mathbf{v}} = 0, \quad (\text{A.1})$$

where $F_{\nu_s}(\mathbf{r}, \mathbf{v})$ is the sterile neutrino distribution at position \mathbf{r} . In the non-relativistic regime, the acceleration $\dot{\mathbf{v}}$ can be obtained through

$$\dot{\mathbf{v}} = \nabla \Phi = -G \int \rho_t \frac{\mathbf{r} - \mathbf{r}'}{|\mathbf{r} - \mathbf{r}'|^3} d^3 r', \quad (\text{A.2})$$

where $\rho_t(r, t)$ is the total energy density of all matters, including cosmological neutrinos and sterile neutrinos, baryons, and cold dark matter. Here, one can divide F_{ν_s} into an unperturbed initial distribution $f_{\nu_s}^0$ plus a gravitational distorted term which is position dependent, $f_{\nu_s}^1(\mathbf{r}, \mathbf{v})$, so that,

$$F_{\nu_s} = f_{\nu_s}^0(\mathbf{v}) + f_{\nu_s}^1(\mathbf{r}, \mathbf{v}). \quad (\text{A.3})$$

For simplicity, we transform the physical coordinates $(t, \mathbf{r}, \mathbf{v})$ into the super-comoving coordinates $(s, \mathbf{x}, \mathbf{u})$ defined as:

$$ds = \frac{dt}{a^2(t)}, \quad \mathbf{x} = \frac{\mathbf{r}}{a(t)}, \quad \mathbf{u} \equiv \frac{d\mathbf{x}}{ds} = a(t)\mathbf{v} - Ha(t)\mathbf{r}. \quad (\text{A.4})$$

The Vlasov equation can be rewritten as

$$\frac{1}{a^2} \frac{\partial F_{\nu_s}}{\partial s} + \frac{\mathbf{u}}{a^2} \cdot \frac{\partial F_{\nu_s}}{\partial \mathbf{u}} - \ddot{a} a \mathbf{x} \cdot \frac{\partial F_{\nu_s}}{\partial \mathbf{u}} + a \mathbf{v} \cdot \frac{\partial F_{\nu_s}}{\partial \mathbf{u}} = 0. \quad (\text{A.5})$$

Combining Eq. (A.2), the Friedmann equation, and Eq. (A.3), Eq. (A.5) can be linearized as

$$\frac{\partial f_{\nu_s}^1}{\partial s} + \mathbf{u} \cdot \frac{\partial f_{\nu_s}^1}{\partial \mathbf{x}} - Ga^4 \frac{\partial f_{\nu_s}^0}{\partial \mathbf{u}} \cdot \int \bar{\rho}_t \delta_t(s, \mathbf{x}') \frac{\mathbf{x} - \mathbf{x}'}{|\mathbf{x} - \mathbf{x}'|^3} d^3x', \quad (\text{A.6})$$

where $\bar{\rho}_t \delta_t \equiv \rho_t - \bar{\rho}_t = \bar{\rho}_{cb} \delta_{cb} + \bar{\rho}_\nu \delta_\nu$. By applying the Fourier transformation and integrating out s from initial time s_i , one can obtain

$$\tilde{f}_{\nu_s}^1(s, \mathbf{k}, \mathbf{u}) + \int_{s_i}^s e^{-i\mathbf{k} \cdot \mathbf{u}(s-s')} 4\pi G a^4 \frac{i\mathbf{k}}{k^2} \frac{f_{\nu_s}^0}{\partial \mathbf{u}} \left[\bar{\rho}_{cb}(s') \tilde{\delta}_{cb}(s', \mathbf{k}) + \bar{\rho}_{\nu_s}(s') \tilde{\delta}_{\nu_s}(s', \mathbf{k}) \right] ds' = \tilde{f}_{\nu_s}^1(s, \mathbf{k}, \mathbf{u}) e^{-i\mathbf{k} \cdot \mathbf{u}(s-s_i)}, \quad (\text{A.7})$$

where $\tilde{\sim}$ denotes the corresponding Fourier transformed variables. Following Ali-Haimoud's work [23], the initial $\tilde{f}_{\nu_s}^1(s_i, \mathbf{k}, \mathbf{u})$ can be expanded by Legendre polynomials

$$\tilde{f}_{\nu_s}^1(s_i, \mathbf{k}, \mathbf{u}) = \sum_{l=0}^{\infty} i^l \tilde{f}_{\nu_s}^{1,(l)}(s_i, \mathbf{k}, \mathbf{u}) P_l(\hat{\mathbf{k}} \cdot \hat{\mathbf{u}}), \quad (\text{A.8})$$

with the coefficients approximated as

$$\begin{aligned} \tilde{f}_{\nu_s}^{1,(0)} &= f_{\nu_s}^0 \tilde{\delta}_{\nu_s}(s_i, \mathbf{k}), \\ \tilde{f}_{\nu_s}^{1,(1)} &= \frac{df_{\nu_s}^0(u)}{du} k^{-1} a_i \tilde{\theta}_{\nu_s}(s_i, \mathbf{k}) = -\frac{df_{\nu_s}^0(u)}{du} k^{-1} a_i^2 H(a_i) \tilde{\delta}_{\nu_s}(s_i, \mathbf{k}), \\ \tilde{f}_{\nu_s}^{1,(l)} &= 0 (l \geq 2), \end{aligned} \quad (\text{A.9})$$

where $\tilde{\theta}_{\nu_s}(s_i, \mathbf{k})$ is the sterile neutrino velocity divergence in k space at initial time. After integrating out \mathbf{u} , the evolution of sterile neutrino over-density δ_{ν_s} follows

$$\begin{aligned} \tilde{\delta}_{\nu_s} &= \tilde{\delta}_{\nu_s}(s_i, \mathbf{k}) \Phi[\mathbf{k}(s-s_i)] \left[1 + (s-s_i) a_i^2 H(a_i) \right] + 4\pi G \int_{s_i}^s a^4 (s-s') \Phi[\mathbf{k}(s-s')] \\ &\quad \times \left[\bar{\rho}_{cb}(s') \delta_{cb}(s', \mathbf{k}) + \sum_i \bar{\rho}_{\nu_i}(s') \delta_{\nu_i}(s', \mathbf{k}) + \bar{\rho}_{\nu_s}(s') \delta_{\nu_s}(s', \mathbf{k}) \right] ds', \end{aligned} \quad (\text{A.10})$$

where $\Phi(\mathbf{q}) \equiv \frac{\int f_{\nu_s}^0 e^{-i\mathbf{q} \cdot \mathbf{u}} d^3\mathbf{u}}{\int f_{\nu_s}^0 d^3\mathbf{u}}$.

A.2 Grid-based Method

Here, the detailed procedure of the simulations is overviewed:

1. The Boltzmann equation solver **CAMB** is used to generate the initial power spectrum of CDM plus baryons and neutrinos. We modify the calculation of the neutrino energy density and pressure so that the mass of neutrinos can be input directly.
2. We generate the initial power spectrum of CDM plus baryons $P_{cb}(k)$ and 3+1 neutrinos $P_\nu(k)$ at redshift $z = 99$. $R_{\text{ini}}(k) \equiv P_{cb}(k)/P_\nu(k)$ is also recorded. In **2LPTic**, $P_{cb}(k)$ is used to generate the initial conditions for our cosmological simulation. We have modified the cosmology so that the effect of neutrinos is included.

3. At the 0th time step of the cosmological simulation, $P_{\text{cb}}(k)$ are calculated with proper binning $\{k_i\}$, so that the initial power spectrum of $3 + 1$ neutrinos are calculated by $P_\nu(k) = P_{\text{cb}}(k)R_{\text{ini}}(k)$. Then, $\tilde{\delta}_{\nu_i}$ and $\tilde{\delta}_{\nu_s}$ estimated from $\tilde{\delta}_\nu(k) = (P_\nu(k))^{1/2}$ are saved as the initial conditions of Eq. (A.10).
4. At the n th time step, the tables of $\tilde{\delta}_{\nu_i}(s, k)$ and $\tilde{\delta}_{\nu_s}(s, k)$ are made for interpolation so that the integration of Eq. (A.10) can be calculated. Then the correction of gravitational potential is obtained by $\Phi = 4\pi G\tilde{\rho}_t(\mathbf{k})$ using Eq. (2.7). Hence, the long-range force on CDM simulation particles includes the neutrino free-streaming effect.

B Refitting of cosmological parameters: different sterile neutrino parameters

Figure 10 displays the MCMC refitting results by Planck 2018 plikHM_TTTEEE and BAO data for fixed m_{phy} and ΔN_{eff} [11, 26]. With a fixed ΔN_{eff} , increasing m_{phy} results in lower Ω_ν and decreases the Hubble parameter H_0 . If one fixes m_{eff} , or sterile neutrino energy density, (see the red and gray contours in Figure 10), increasing ΔN_{eff} indeed alleviates the Hubble tension. It is shown that both Ω_m and σ_8 are only sensitive to m_{eff} . One can alleviate the S8 tension by increasing m_{eff} .

C Cosmic variance

This paper uses a random seed value of 667788 for our simulations. Additionally, we run simulations with a different random seed value of 271828 to evaluate the stability of the sterile neutrino effect. Here, we take the fractional deviation of the matter power spectrum as an example.

Figure 11 shows the results with solid and dashed lines representing the random seeds 667788 and 271828, respectively. we find the fractional deviations with respect to their corresponding fiducial A0 case show only small cosmic variance. Such stability can be also found when varying ΔN_{eff} with fixed m_{phy} . Consequently, this paper uses the random seed value of 667788.

Acknowledgments

The computational resources used in this work were kindly provided by the Chinese University of Hong Kong Central Research Computing Cluster. Furthermore, this research is supported by grants from the Research Grants Council of the Hong Kong Special Administrative Region, China, under Project No.s AoE/P-404/18 and 14300223. All plots in this paper are generated by Matplotlib [66]. We also use NumPy [67], SciPy [68] and Pandas [69].

References

- [1] M. Goldhaber, L. Grodzins and A.W. Sunyar, *Helicity of Neutrinos*, *Phys. Rev.* **109** (1958) 1015.
- [2] S. Gariazzo, C. Giunti, M. Laveder, Y.F. Li and E.M. Zavatin, *Light sterile neutrinos*, *J. Phys. G* **43** (2016) 033001 [1507.08204].
- [3] R.N. Mohapatra, S. Nasri and H.-B. Yu, *Seesaw right handed neutrino as the sterile neutrino for LSND*, *Phys. Rev. D* **72** (2005) 033007 [hep-ph/0505021].

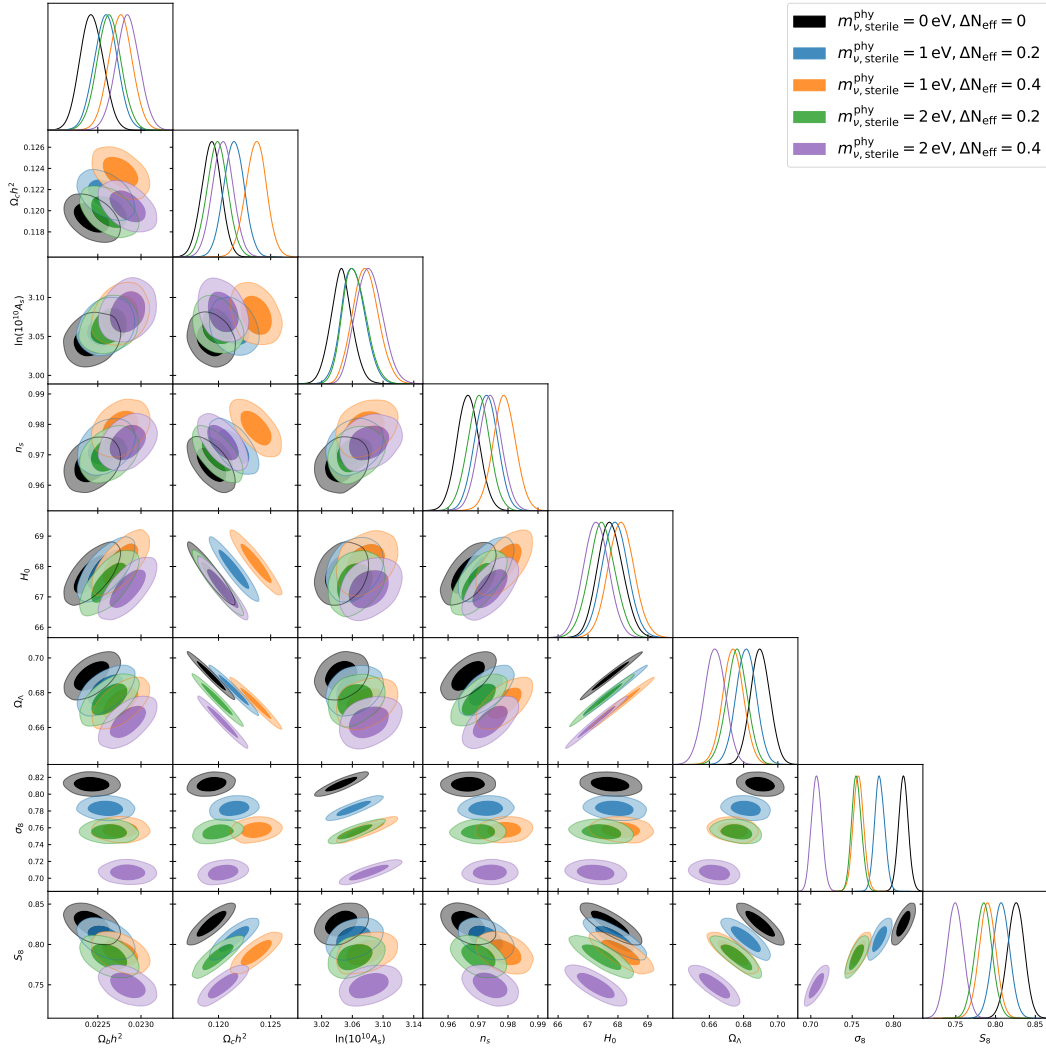


Figure 10. 1D posterior PDFs and 2D contours of selected cosmological parameters obtained by MCMC refitting of Planck data and BAO data with different sterile neutrino parameters (shown by colors). The lighter and darker shadow regions show the 2D contour for 95% C.L. and 68% C.L., respectively.

- [4] K.N. Abazajian et al., *Light Sterile Neutrinos: A White Paper*, [1204.5379](#).
- [5] LSND collaboration, *Evidence for $\nu_\mu \rightarrow \nu_e$ neutrino oscillations from LSND*, *Phys. Rev. Lett.* **81** (1998) 1774 [[nucl-ex/9709006](#)].
- [6] MINIBOONE collaboration, *Significant Excess of ElectronLike Events in the MiniBooNE Short-Baseline Neutrino Experiment*, *Phys. Rev. Lett.* **121** (2018) 221801 [[1805.12028](#)].
- [7] MINOS, MINOS+, DAYA BAY, BUGEY-3 collaboration, *Improved Limits on Sterile Neutrino Mixing from a Joint Search of the MINOS, MINOS+, Daya Bay, and Bugey-3 Experiments*, *PoS ICHEP2020* (2021) 201.
- [8] MICROBOONE collaboration, *First Constraints on Light Sterile Neutrino Oscillations from Combined Appearance and Disappearance Searches with the MicroBooNE Detector*, *Phys. Rev. Lett.* **130** (2023) 011801 [[2210.10216](#)].

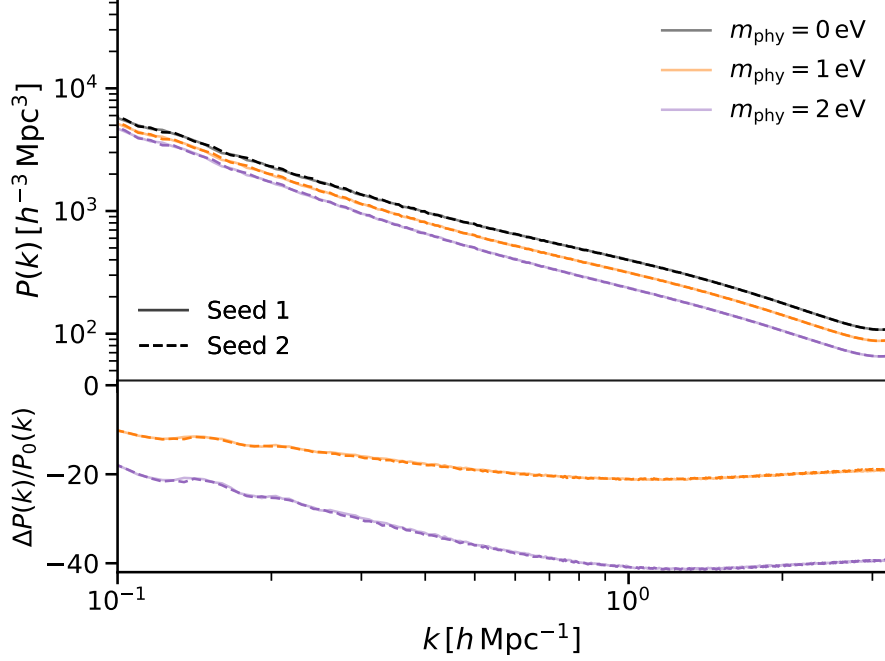


Figure 11. Total matter power spectra (upper panel) and their fractional deviations (lower panel) with respect to the fiducial A0 case for different m_{phy} with two different random seeds: 667788 (solid lines) and 271828 (dashed lines). A fixed value of $\Delta N_{\text{phy}} = 0.4$ is used for all curves.

- [9] J.J. Bennett, G. Buldgen, P.F. De Salas, M. Drewes, S. Gariazzo, S. Pastor et al., *Towards a precision calculation of N_{eff} in the Standard Model II: Neutrino decoupling in the presence of flavour oscillations and finite-temperature QED*, *JCAP* **04** (2021) 073 [2012.02726].
- [10] J. Froustey, C. Pitrou and M.C. Volpe, *Neutrino decoupling including flavour oscillations and primordial nucleosynthesis*, *JCAP* **12** (2020) 015 [2008.01074].
- [11] PLANCK collaboration, *Planck 2018 results. VI. Cosmological parameters*, *Astron. Astrophys.* **641** (2020) A6 [1807.06209].
- [12] S. Dodelson and L.M. Widrow, *Sterile-neutrinos as dark matter*, *Phys. Rev. Lett.* **72** (1994) 17 [hep-ph/9303287].
- [13] A.-K. Burns, T.M.P. Tait and M. Valli, *Indications for a Nonzero Lepton Asymmetry from Extremely Metal-Poor Galaxies*, *Phys. Rev. Lett.* **130** (2023) 131001 [2206.00693].
- [14] J. Lesgourgues, G. Mangano, G. Miele and S. Pastor, *Neutrino Cosmology*, Cambridge University Press (2, 2013).
- [15] L. Miller et al., *Bayesian Galaxy Shape Measurement for Weak Lensing Surveys - III. Application to the Canada-France-Hawaii Telescope Lensing Survey*, *Mon. Not. Roy. Astron. Soc.* **429** (2013) 2858 [1210.8201].
- [16] eBOSS collaboration, *The Completed SDSS-IV Extended Baryon Oscillation Spectroscopic Survey: Baryon Acoustic Oscillations with Ly α Forests*, *Astrophys. J.* **901** (2020) 153 [2007.08995].
- [17] A. Vikhlinin et al., *Chandra Cluster Cosmology Project II: Samples and X-ray Data Reduction*, *Astrophys. J.* **692** (2009) 1033 [0805.2207].

- [18] M. Costanzi, B. Sartoris, M. Viel and S. Borgani, *Neutrino constraints: what large-scale structure and CMB data are telling us?*, *JCAP* **10** (2014) 081 [[1407.8338](#)].
- [19] L. Amendola et al., *Cosmology and fundamental physics with the Euclid satellite*, *Living Rev. Rel.* **21** (2018) 2 [[1606.00180](#)].
- [20] DESI collaboration, *The DESI Experiment, a whitepaper for Snowmass 2013*, [1308.0847](#).
- [21] CORE collaboration, *Exploring cosmic origins with CORE: Cosmological parameters*, *JCAP* **04** (2018) 017 [[1612.00021](#)].
- [22] C.B.d.S. Nascimento and M. Loverde, *Neutrinos in N-body simulations*, *Phys. Rev. D* **104** (2021) 043512 [[2102.05690](#)].
- [23] Y. Ali-Haimoud and S. Bird, *An efficient implementation of massive neutrinos in non-linear structure formation simulations*, *Mon. Not. Roy. Astron. Soc.* **428** (2012) 3375 [[1209.0461](#)].
- [24] J.Z. Chen, A. Upadhye and Y.Y.Y. Wong, *One line to run them all: SuperEasy massive neutrino linear response in N-body simulations*, *JCAP* **04** (2021) 078 [[2011.12504](#)].
- [25] S. Agarwal and H.A. Feldman, *The effect of massive neutrinos on the matter power spectrum*, *Mon. Not. Roy. Astron. Soc.* **410** (2011) 1647 [[1006.0689](#)].
- [26] W.J. Percival, S. Cole, D.J. Eisenstein, R.C. Nichol, J.A. Peacock, A.C. Pope et al., *Measuring the Baryon Acoustic Oscillation scale using the SDSS and 2dFGRS*, *Mon. Not. Roy. Astron. Soc.* **381** (2007) 1053 [[0705.3323](#)].
- [27] BOSS collaboration, *The clustering of galaxies in the completed SDSS-III Baryon Oscillation Spectroscopic Survey: Observational systematics and baryon acoustic oscillations in the correlation function*, *Mon. Not. Roy. Astron. Soc.* **464** (2017) 1168 [[1607.03145](#)].
- [28] Y.P. Jing, H.J. Mo and G. Borner, *Spatial correlation function and pairwise velocity dispersion of galaxies: CDM models versus the Las Campanas Survey*, *Astrophys. J.* **494** (1998) 1 [[astro-ph/9707106](#)].
- [29] 2dFGRS collaboration, *The 2dF Galaxy Redshift Survey: Power-spectrum analysis of the final dataset and cosmological implications*, *Mon. Not. Roy. Astron. Soc.* **362** (2005) 505 [[astro-ph/0501174](#)].
- [30] Z. Zhai, J.L. Tinker, A. Banerjee, J. DeRose, H. Guo, Y.-Y. Mao et al., *The Aemulus Project. V. Cosmological Constraint from Small-scale Clustering of BOSS Galaxies*, *Astrophys. J.* **948** (2023) 99 [[2203.08999](#)].
- [31] Y.-Z. Ma, M. Li and P. He, *Constraining cosmology with pairwise velocity estimator*, *Astron. Astrophys.* **583** (2015) A52 [[1509.06413](#)].
- [32] R. Juszkiewicz, P.G. Ferreira, H.A. Feldman, A.H. Jaffe and M. Davis, *Evidence for a low density universe from the relative velocities of galaxies*, *Science* **287** (2000) 109 [[astro-ph/0001041](#)].
- [33] H.A. Feldman et al., *An estimate of ω_m without priors*, *Astrophys. J. Lett.* **596** (2003) L131 [[astro-ph/0305078](#)].
- [34] W. Zhang, M.-c. Chu, S. Liao, S. Yeung and H.-J. Hu, *Measuring the Hubble Constant through the Galaxy Pairwise Peculiar Velocity*, *Astrophys. J. Lett.* **978** (2025) L6 [[2412.04660](#)].
- [35] M. Jaber, W.A. Hellwing, J.E. García-Farieta, S. Gupta and M. Bilicki, *Dynamics of pairwise motions in the fully nonlinear regime in LCDM and modified gravity cosmologies*, *Phys. Rev. D* **109** (2024) 123528 [[2312.00472](#)].
- [36] S. Bhattacharya and A. Kosowsky, *Cosmological Constraints from Galaxy Cluster Velocity Statistics*, *Astrophys. J. Lett.* **659** (2007) L83 [[astro-ph/0612555](#)].
- [37] R.K. Sheth, *The Distribution of pairwise peculiar velocities in the nonlinear regime*, *Mon. Not. Roy. Astron. Soc.* **279** (1996) 1310 [[astro-ph/9511068](#)].

- [38] R.K. Sheth, L. Hui, A. Diaferio and R. Scoccimarro, *Linear and nonlinear contributions to pairwise peculiar velocities*, *Mon. Not. Roy. Astron. Soc.* **325** (2001) 1288 [[astro-ph/0009167](#)].
- [39] H. Mo, Y. Jing and G. Börner, *On the pairwise velocity dispersion of galaxies*, *Mon. Not. Roy. Astron. Soc.* **264** (1993) 825.
- [40] W. Zhang, M.-c. Chu, R. Hu, S. Liao and S. Yeung, *Measuring neutrino mass and asymmetry with matter pairwise velocities*, *Mon. Not. Roy. Astron. Soc.* **529** (2024) 360 [[2312.04278](#)].
- [41] W. Cui, S. Borgani, K. Dolag, G. Murante and L. Tornatore, *The effects of baryons on the halo mass function*, *Mon. Not. Roy. Astron. Soc.* **423** (2012) 2279 [[1111.3066](#)].
- [42] R. Stanek, D. Rudd and A.E. Evrard, *The Effect of Gas Physics on the Halo Mass Function*, *Mon. Not. Roy. Astron. Soc.* **394** (2009) L11 [[0809.2805](#)].
- [43] E. Castorina, E. Sefusatti, R.K. Sheth, F. Villaescusa-Navarro and M. Viel, *Cosmology with massive neutrinos II: on the universality of the halo mass function and bias*, *JCAP* **02** (2014) 049 [[1311.1212](#)].
- [44] C.S. Kochanek, *Dynamical probes of the halo mass function*, [astro-ph/0108160](#).
- [45] I. Zehavi, S.E. Kerby, S. Contreras, E. Jiménez, N. Padilla and C.M. Baugh, *On the prospect of using the maximum circular velocity of halos to encapsulate assembly bias in the galaxy-halo connection*, *Astrophys. J.* **887** (2019) 17 [[1907.05424](#)].
- [46] A.H. Gonzalez, K.A. Williams, J.S. Bullock, T.S. Kolatt and J.R. Primack, *The velocity function of galaxies*, *Astrophys. J.* **528** (2000) 145 [[astro-ph/9908075](#)].
- [47] S. Gariazzo, P.F. de Salas and S. Pastor, *Thermalisation of sterile neutrinos in the early Universe in the 3+1 scheme with full mixing matrix*, *JCAP* **07** (2019) 014 [[1905.11290](#)].
- [48] Z. Zeng, S. Yeung and M.-C. Chu, *Effects of neutrino mass and asymmetry on cosmological structure formation*, *JCAP* **03** (2019) 015 [[1808.00357](#)].
- [49] V. Springel, *The Cosmological simulation code GADGET-2*, *Mon. Not. Roy. Astron. Soc.* **364** (2005) 1105 [[astro-ph/0505010](#)].
- [50] M. Crocce, S. Pueblas and R. Scoccimarro, *Transients from Initial Conditions in Cosmological Simulations*, *Mon. Not. Roy. Astron. Soc.* **373** (2006) 369 [[astro-ph/0606505](#)].
- [51] A. Lewis, A. Challinor and A. Lasenby, *Efficient computation of CMB anisotropies in closed FRW models*, *Astrophys. J.* **538** (2000) 473 [[astro-ph/9911177](#)].
- [52] A. Lewis and S. Bridle, *Cosmological parameters from CMB and other data: A Monte Carlo approach*, *Phys. Rev. D* **66** (2002) 103511 [[astro-ph/0205436](#)].
- [53] P.S. Behroozi, R.H. Wechsler and H.-Y. Wu, *The Rockstar Phase-Space Temporal Halo Finder and the Velocity Offsets of Cluster Cores*, *Astrophys. J.* **762** (2013) 109 [[1110.4372](#)].
- [54] F. Villaescusa-Navarro, “Pylans: Python libraries for the analysis of numerical simulations.” Astrophysics Source Code Library, record ascl:1811.008, Nov., 2018.
- [55] S.D. Landy and A.S. Szalay, *Bias and variance of angular correlation functions*, *Astrophys. J.* **412** (1993) 64.
- [56] P.G. Ferreira, R. Juszkiewicz, H.A. Feldman, M. Davis and A.H. Jaffe, *Streaming velocities as a dynamical estimator of omega*, *Astrophys. J. Lett.* **515** (1999) L1 [[astro-ph/9812456](#)].
- [57] H. Mo, F.C. van den Bosch and S. White, *Galaxy Formation and Evolution* (2010).
- [58] E.V. Linder, *Cosmic growth history and expansion history*, *Phys. Rev. D* **72** (2005) 043529 [[astro-ph/0507263](#)].
- [59] R.K. Sheth and G. Tormen, *Large scale bias and the peak background split*, *Mon. Not. Roy. Astron. Soc.* **308** (1999) 119 [[astro-ph/9901122](#)].

- [60] C. Hernández-Aguayo et al., *The MillenniumTNG Project: Impact of massive neutrinos on the cosmic large-scale structure and the distribution of galaxies*, [2407.21103](#).
- [61] C. Conroy, R.H. Wechsler and A.V. Kravtsov, *Modeling luminosity-dependent galaxy clustering through cosmic time*, *Astrophys. J.* **647** (2006) 201 [[astro-ph/0512234](#)].
- [62] A. Klypin, S. Trujillo-Gomez and J. Primack, *Dark matter halos in the standard cosmological model: results from the Bolshoi simulation*, *Astrophys. J.* **740** (2011) 102 [[1002.3660](#)].
- [63] S. Trujillo-Gomez, A. Klypin, J. Primack and A.J. Romanowsky, *Galaxies in LCDM with Halo Abundance Matching: luminosity-velocity relation, baryonic mass-velocity relation, velocity function and clustering*, *Astrophys. J.* **742** (2011) 16 [[1005.1289](#)].
- [64] A. Notari, F. Rompineve and G. Villadoro, *Improved Hot Dark Matter Bound on the QCD Axion*, *Phys. Rev. Lett.* **131** (2023) 011004 [[2211.03799](#)].
- [65] H.W. Wong and M.-c. Chu, *Effects of neutrino masses and asymmetries on dark matter halo assembly*, *JCAP* **03** (2022) 066 [[2109.00303](#)].
- [66] J.D. Hunter, *Matplotlib: A 2D Graphics Environment*, *Computing in Science and Engineering* **9** (2007) 90.
- [67] C.R. Harris et al., *Array programming with NumPy*, *Nature* **585** (2020) 357 [[2006.10256](#)].
- [68] P. Virtanen et al., *SciPy 1.0—Fundamental Algorithms for Scientific Computing in Python*, *Nature Meth.* **17** (2020) 261 [[1907.10121](#)].
- [69] W. McKinney, *Data Structures for Statistical Computing in Python*, 2010, [DOI](#).